Cosmogenic isotopes Be-7, Be-10, C-14, Na-22 and Cl-36 in the atmosphere: Altitudinal profiles of yield functions

Stepan Poluianov[*]

Space Climate Research Unit, University of Oulu, Finland
Sodankylä Geophysical Observatory, University of Oulu, Finland
E-mail: stepan.poluianov@oulu.fi

Gennady Kovaltsov

Ioffe Physical-Technical Institute, St. Petersburg, Russia

Alexander Mishev

Space Climate Research Unit, University of Oulu, Finland

Ilya Usoskin

Space Climate Research Unit, University of Oulu, Finland
Sodankylä Geophysical Observatory, University of Oulu, Finland

Production of isotopes by cosmic rays in the Earth's atmosphere plays a key role in many studies in solar physics, geophysics, archeology and other fields. For those purposes, precise quantitative modeling of their production is crucial, and high-resolution altitudinal profiles of production rates are in high demand. Here we present detailed and consistent yield functions of isotopes ^{7}Be, ^{10}Be, ^{14}C, ^{22}Na and ^{36}Cl produced by energetic particles in the atmosphere. Comparison of reconstructions of the ^{10}Be deposition flux in 1951-2013 and around 775 AD with ice core measurements is shown for illustration of application of our yield functions.

---

[*]Speaker.

1. Introduction

The Earth's atmosphere is constantly bombarded by cosmic ray particles. They are sufficiently energetic to induce cascades of nuclear reactions in air. Some species of such a cascade can interact with atmospheric nitrogen, oxygen, argon and produce so-called cosmogenic isotopes. Those products can be measured directly in the atmosphere or in natural paleoclimatic archives (e.g, tree trunks, ice cores, etc.) and provide a lot of useful information for solar-, space-, atmospheric physics, archaeology and other fields of science [3].

Reliable quantitative modelling of the nuclide production requires extensive Monte Carlo computations for simulation of the cosmic ray cascade. The yield function approach became standard for that purpose because it allows to pre-compute the production of a nuclide irrespective of the energy spectrum of primary particles. Then, using a relatively simple equation, one can calculate the nuclide production by any particles' spectrum of interest. Yield functions for most important isotopes have been computed and published earlier with different assumptions and conditions [e.g., 9, 10, 12, 14, 30, 31]. Their high altitudinal resolution is important as an input of realistic atmospheric transport models, but previously published yield functions were either without or very rough altitudinal resolution.

Here we present detailed altitudinal profiles of new consistent yield functions for cosmogenic isotopes ^{7}Be, ^{10}Be, ^{14}C, ^{22}Na and ^{36}Cl, which are the most important for space- and atmospheric physics. Their tabulated values are published in the supplementary material of [21].

2. Concept of the yield function

3. Definition

The yield function $Y(E,h)$ is the number of atoms of a given nuclide produced at the depth h (in g/cm^2) per the unit mass of air (in g) by the unit intensity of primary energetic particles of the ith type with the energy per nucleon E. The units of $Y(E,h)$ are (atoms sr cm^2)/g. Thus, the nuclide production rate $Q(h)$ (in atoms/(s g)) can be computed as:

$$Q(h) = \sum_i \int_{E_i^{cutoff}}^{\infty} Y_i(E,h)J_i(E)dE, \qquad (3.1)$$

where i is the type index of primary particles (protons and α-particles), E_i^{cutoff} is the energy of the geomagnetic cutoff (in MeV) and $J_i(E)$ is their differential flux (in primaries/(cm^2 sr s MeV)).

The yield function $Y(E,h)$ is often presented in the form of the so-called production function $S(E,h)$, which is the direct result of computations and can be described as production of the isotope by one primary particle hitting the top of the atmosphere [30]. For the isotropic cosmic ray flux, the relation between the yield and production functions is

$$Y = \pi S, \qquad (3.2)$$

where π is conversion factor from flux at the top of the atmosphere (particles/cm^2 s) to the cosmic ray intensity in the interplanetary space (particles/cm^2 sr s).

3.1 Calculation of the yield function

The calculation of yield functions is based on Monte Carlo simulation of the nucleonic component of the cosmic ray cascade in the atmosphere. For that purpose we used the toolkit GEANT4.10.0 [1, 2]. The atmosphere was modelled as a set of spherical layers with the realistic size. The top of the atmosphere was set at 100 km. Each layer had homogeneous properties and the thickness from 1 (top layers) to 50 g/cm^2 (bottom layers). The total thickness of the atmosphere was 1050 g/cm^2, and soil was not included into the model. The composition of layers was set according to the model NRLMSISE-2000 [20].

We calculated yield functions for isotropically distributed cosmic ray protons and α-particles, assuming that heavier species can be scaled from α-particles. The GEANT4 model has been run over a quasilogarithmic energy grid of primaries (0.02–100 GeV/nuc).

The results of simulations were the numbers of secondary particles able to produce the nuclide (protons, neutrons and α-particles) weighted with $|\cos\theta|$ (where θ is the zenith angle), stored in depth-energy histograms. Those data divided by the energy bin width $\Delta E'$ correspond to the quantity $F_k(h, E, E')$ (in units 1/MeV), where k is the index of the type of secondary particles, E' is the energy of secondary particles and E is the energy per nucleon of primary particles. The production function then is

$$S(E, h) = \sum_j \sum_k \int k_j F_k(h, E, E') \sigma_{j,k}(E') dE, \qquad (3.3)$$

where j is the index of target nuclei, k_j is the content of jth target nuclei (atoms/g) and $\sigma_{j,k}(E')$ is the cross-section of the corresponding nuclear reactions. We adopted the cross-section data from [3, 8, 11, 22, 24, 31] and also from the Experimental Nuclear Reaction Database (EXFOR/CSISRS) [19]. Transport of neutrons with the energies below 1 keV that is, in particular, important for production of ^{14}C, was calculated according to [9].

The results of computation $S(h)$ are published in the supplementary material of [21] as tabulated values. Several altitudinal profiles of the ^{36}C production function for primary protons are shown in Figure 1 for illustration of the results. For relatively low energies (the left panel A of the figure), ^{36}Cl is produced mostly by spallation of argon by primaries in the top atmospheric layer of several tens of g/cm^2. Primaries with higher energies (the right panel B of the figure) are able to initiate a developed cascade in air, and the production of ^{36}Cl by secondaries extends to much deeper layers of the atmosphere.

4. Nuclide production

4.1 Columnar production functions

Since yield/production functions have been often published and discussed as columnar values [9, 30], for comparison with those results we computed our production functions integrated over the height of the atmosphere.The columnar production functions for ^{7}Be by protons and α-particles are shown in Figure 2. One can see that presenting here results (the solid curve) are in good agreement with the functions published earlier [27, 30].
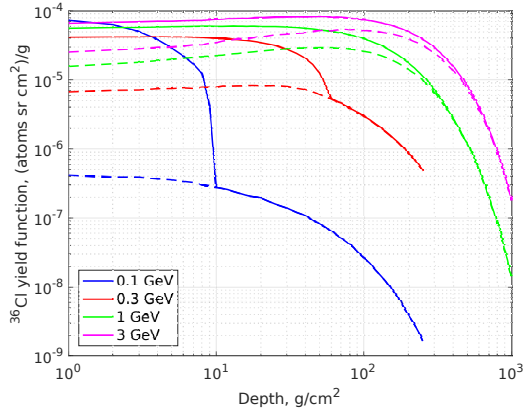
Figure 1: Altitudinal profiles of the ^{36}Cl production functions by primary protons with the energies denoted in the legend. The doted lines correspond to the contribution from secondary neutrons.

4.2 Global production rate

As another illustration of our results, we calculated the globally averaged production rates Q_{global} (atoms/(cm^2 s)) of considered here isotopes by galactic cosmic rays according to the following equation:

$$Q_{global}(\phi) =$$
$$= \frac{1}{4\pi} \int_\Omega \int_h Q(\phi, h, P_{cutoff}(\Omega, M)) dh d\Omega,$$
$$(4.1)$$

where $Q(\phi, h, P_{cutoff}(\Omega, M))$ is the produc-

Figure 2: Columnar production $S_{columnar}(E)$ of ^{7}Be by primary protons and α-particles. Usoskin2008 and Webber2007 indicate [27] and [30], respectively.

tion rate defined by equation 3.1, M is the Earth's magnetic dipole moment, which slowly varies in time within $(6–12) \cdot 10^{22}$ A·m^2 [e.g., 6, 18]. Its present value is about $7.8 \cdot 10^{22}$ A·m^2. The intensity of the geomagnetic field is important for the effectiveness of the shielding and affects the geomagnetic cutoff rigidity $P_{cutoff}(\Omega, M)$, which is also a function of geographical coordinates. The modulation potential ϕ parametrizes the differential flux of galactic cosmic rays $J(E, \phi)$ at 1 AU (in equation 3.1). The approach is described elsewhere [e.g., 29, 31]. Here we use the modulation potential defined similarly to [28] with the local interstellar spectrum as in [5].

The global production rates $Q_{global}(\phi)$ for ^{7}Be, ^{10}Be, ^{14}C, ^{22}Na, ^{36}Cl calculated for several values of M are shown in Figure 3. One can see that both parameters responsible for the cosmic ray flux at the top of the atmosphere (ϕ and M) play important roles in the production rates of the nuclides. The global production rates for ^{7}Be, ^{10}Be, ^{14}C and ^{22}Na presented here are in good agreement (within 5%) with those published by us earlier [9, 10, 12, 27] computed with the CRAC model. The global production rate of nuclide ^{36}Cl match the value calculated by [14] within the discrepancy of 15%.
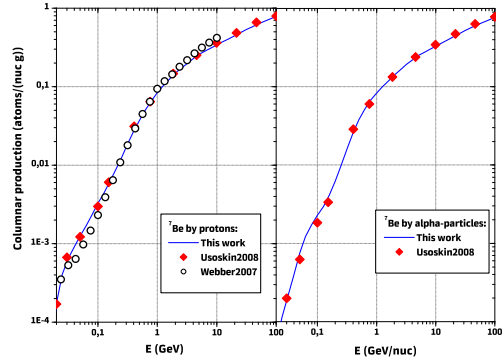
We note that the globally averaged production rate makes sense only for ^{14}C, which is well mixed in the atmosphere over the globe. Other isotopes (^{7}Be, ^{10}Be, ^{22}Na, ^{36}Cl) are more dependent on regional transport and deposition processes, thus, it seems to be unreasonable to use those global production rates in practice.

5. Verification

For verification of our results, we computed the time series of ^{10}Be deposition flux in the northern polar region and compared it with ^{10}Be measurements in the Greenland NGRIP ice core [4].

Figure 3: Global production rates of ^{7}Be, ^{10}Be, ^{14}C, ^{22}Na and ^{36}Cl by galactic cosmic rays as a function of the modulation potential ϕ and geomagnetic dipole moment M.

The estimated deposition flux of ^{10}Be is based on the production rate by galactic cosmic rays obtained from the presented here yield functions and the modulation potential ϕ reconstructed from neutron monitor data [28]. We applied the atmospheric transport model by [7] and one year delay caused by residence of ^{10}Be in air. The modelled result is in good agreement with measurements (Figure 4), especially for the period of 1951–1970, thus, it verifies the yield function of ^{10}Be presented in this work.
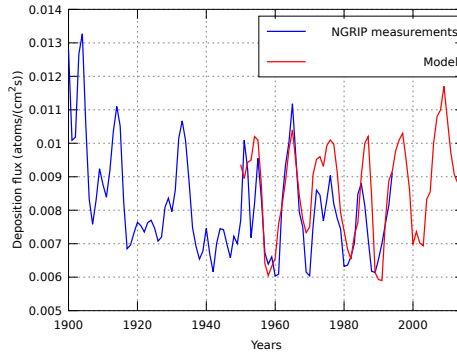

Figure 4: Deposition flux of ^{10}Be during last decades. The blue curve corresponds to the measurements of ^{10}Be in the NGRIP ice core in Greenland [4], the red one represents the results of our production model (the transport model from [7]). The data are smoothed.

Another example of application of our production model is related to the strongest known solar energetic particle event that took place in 775 A.D. [15, 16, 25]. Not discussing the event itself, we use the opportunity to compare the decadal-mean deposition flux of ^{10}Be with several measurements of that nuclide in natural archives in samples corresponding to the period around that date. Figure 5 shows the ^{10}Be deposition flux as a function of the modulation potential ϕ for the polar regions of the northern and southern hemispheres (black solid and doted curves). It was calculated assuming the geomagnetic dipole moment $M = 10^{23}$ A·m^2 [13] and the atmospheric
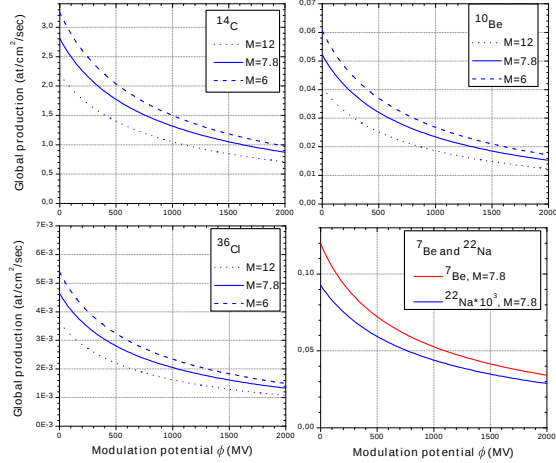
transport model by [7]. The blue horizontal stripe represents the measurements of ^{10}Be in ice cores from Antarctica and Greenland for the period 780–800 A.D[17, 23]. The red vertical stripe indicates the range of the modulation potential ϕ reconstructed from ^{14}C for the period 780–790 A.D. [26]. The modelled deposition flux of ^{10}Be matches the crossing of the two stripes (reconstructed ϕ and measurements of ^{10}Be). This confirms the reliability of the ^{10}Be yield function presented in this work.

6. Summary

We have calculated a new consistent and precise set of yield functions for cosmogenic isotopes ^{7}Be, ^{10}Be, ^{14}C, ^{22}Na and ^{36}Cl produced by cosmic rays in the Earth's atmosphere. The yield functions have high altitudinal and energy resolution, which is important for modelling of their transport and consequent applications. The results are presented as tabulated production functions in the supplementary material of the publication [21]. The values are in good agreement with earlier works and, in particular, ^{10}Be data are also confirmed by comparison with ^{10}Be deposition flux during last decades measured in Greenland NGRIP ice core and for the period around 780 AD.

Figure 5: Deposition flux of ^{10}Be in the northern and southern polar regions computed with our production model (the transport model by [7]) for the geomagnetic dipole moment $M = 10^{23}$ A·m^2 corresponding to the period 780–790 A.D [13]. The horizontal stripe represents the measurements of ^{10}Be in ice cores from Antarctica and Greenland for the period 780–800 A.D. [17, 23]. The vertical stripe indicates the range of the modulation potential ϕ reconstructed from ^{14}C for the period 780–790 A.D. [26].

References

[1] S. Agostinelli, J. Allison, K. Amako, et al. Geant4 - a simulation toolkit. *Nucl. Instr. Meth. Phys. A*, 506(3):250–303, 2003.

[2] J. Allison, K. Amako, J. Apostolakis, et al. Geant4 developments and applications. *Nuclear Science, IEEE Transactions on*, 53(1):270–278, Feb 2006.

[3] J. Beer, K. McCracken, and R. von Steiger. *Cosmogenic Radionuclides: Theory and Applications in the Terrestrial and Space Environments*. Springer, Berlin, 2012.

[4] A.-M. Berggren, J. Beer, G. Possnert, A. Aldahan, P. Kubik, M. Christl, S. J. Johnsen, J. Abreu, and B. M. Vinther. A 600-year annual ^{10}Be record from the NGRIP ice core, Greenland. *Geophys. Res. Lett.*, 36:L11801, June 2009.

[5] R.A. Burger, M.S. Potgieter, and B. Heber. Rigidity dependence of cosmic ray proton latitudinal gradients measured by the ulysses spacecraft: Implications for the diffusion tensor. *J. Geophys. Res.*, 105:27447–27456, 2000.
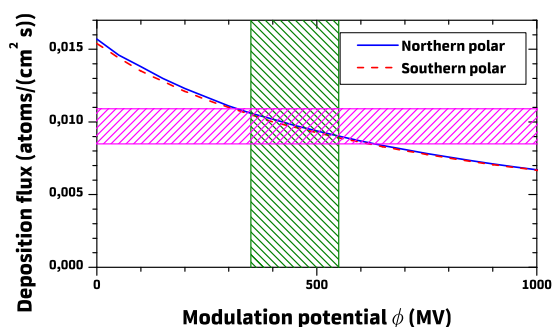
[6] A. Genevey, Y. Gallet, C. G. Constable, M. Korte, and G. Hulot. ArcheoInt: An upgraded compilation of geomagnetic field intensity data for the past ten millennia and its application to the recovery of the past dipole moment. *Geochem., Geophys., Geosyst.*, 9:Q04038, 2008.

[7] U. Heikkilä, J. Beer, and J. Feichter. Meridional transport and deposition of atmospheric ^{10}Be. *Atmos. Chem. Phys.*, 9:515–527, January 2009.

[8] A.J.T. Jull, S. Cloudt, D.J. Donahue, J.M. Sisterson, R.C. Reedy, and J. Masarik. 14c depth profiles in apollo 15 and 17 cores and lunar rock 68815. *Geochimica et Cosmochimica Acta*, 62(17):3025–3036, 1998.

[9] G. A. Kovaltsov, A. Mishev, and I. G. Usoskin. A new model of cosmogenic production of radiocarbon ^{14}C in the atmosphere. *Earth Planet. Sci. Lett.*, 337:114–120, July 2012.

[10] G. A. Kovaltsov and I. G. Usoskin. A new 3D numerical model of cosmogenic nuclide ^{10}Be production in the atmosphere. *Earth Planet. Sci. Lett.*, 291:182–188, March 2010.

[11] H.-J. Lange, T. Hahn, R. Michel, T. Schiekel, R. Rãűsel, U. Herpers, H.-J. Hofmann, B. Dittrich-Hannen, M. Suter, W. Wãűlfli, and P.W. Kubik. Production of residual nuclei by Îś-induced reactions on c, n, o, mg, al and si up to 170 mev. *Applied Radiation and Isotopes*, 46(2):93 – 112, 1995.

[12] A.-P. Leppänen, I. G. Usoskin, G. A. Kovaltsov, and J. Paatero. Cosmogenic ^{7}Be and ^{22}Na in Finland: Production, observed periodicities and the connection to climatic phenomena. *Journal of Atmospheric and Solar-Terrestrial Physics*, 74:164–180, January 2012.

[13] A. Licht, G. Hulot, Y. Gallet, and E. Thébault. Ensembles of low degree archeomagnetic field models for the past three millennia. *Physics of the Earth and Planetary Interiors*, 224:38–67, November 2013.

[14] J. Masarik and J. Beer. An updated simulation of particle fluxes and cosmogenic nuclide production in the Earth's atmosphere. *J. Geophys. Res.*, 114:D11103, 2009.

[15] F. Mekhaldi, R. Muscheler, F. Adolphi, A. Aldahan, J. Beer, J. R. McConnell, G. Possnert, M. Sigl, A. Svensson, H.-A. Synal, K. C. Welten, and T. E. Woodruff. Multiradionuclide evidence for the solar origin of the cosmic-ray events of #7424#7429 774/5 and 993/4. *Nature Communications*, 6:8611, October 2015.

[16] F. Miyake, K. Nagaya, K. Masuda, and T. Nakamura. A signature of cosmic-ray increase in AD 774-775 from tree rings in Japan. *Nature*, 486:240–242, June 2012.

[17] F. Miyake, A. Suzuki, K. Masuda, K. Horiuchi, H. Motoyama, H. Matsuzaki, Y. Motizuki, K. Takahashi, and Y. Nakai. Cosmic ray event of A.D. 774-775 shown in quasi-annual ^{10}Be data from the Antarctic Dome Fuji ice core. *Geophys. Res. Lett.*, 42:84–89, January 2015.

[18] A. Nilsson, R. Holme, M. Korte, N. Suttie, and M. Hill. Reconstructing Holocene geomagnetic field variation: new methods, models and implications. *Geophysical Journal International*, 198:229–248, July 2014.

[19] N. Otuka, E. Dupont, V. Semkova, et al. Towards a more complete and accurate experimental nuclear reaction data library (exfor): International collaboration between nuclear reaction data centres (nrdc). *Nuclear Data Sheets*, 120:272 – 276, 2014.

[20] J. M. Picone, A. E. Hedin, D. P. Drob, and A. C. Aikin. Nrlmsise-00 empirical model of the atmosphere: Statistical comparisons and scientific issues. *J. Geophys. Res.: Space Phys.*, 107(A12):SIA 15–1–SIA 15–16, 2002. 1468.

[21] S. V. Poluianov, G. A. Kovaltsov, A. L. Mishev, and I. G. Usoskin. Production of cosmogenic isotopes ^{7}Be, ^{10}Be, ^{14}C, ^{22}Na, and ^{36}Cl in the atmosphere: Altitudinal profiles of yield functions. *Journal of Geophysical Research (Atmospheres)*, 121:8125–8136, July 2016.

[22] J.-L. Reyss, Y. Yokoyama, and F. Guichard. Production cross sections of Al-26, Na-22, Be-7 from argon and of Be-10, Be-7 from nitrogen - Implications for production rates of Al-26 and Be-10 in the atmosphere. *Earth and Planetary Science Letters*, 53:203–210, April 1981.

[23] M. Sigl, M. Winstrup, J. R. McConnell, et al. Timing and climate forcing of volcanic eruptions for the past 2,500 years. *Nature*, 523:543–549, July 2015.

[24] V. Tatischeff, B. Kozlovsky, J. Kiener, and R. J. Murphy. Delayed X- and Gamma-Ray Line Emission from Solar Flare Radioactivity. *Astrophys. J. Suppl.*, 165:606–617, August 2006.

[25] I. G. Usoskin. A history of solar activity over millennia. *Living Reviews in Solar Physics*, 14:3, March 2017.

[26] I. G. Usoskin, Y. Gallet, F. Lopes, G. A. Kovaltsov, and G. Hulot. Solar activity during the Holocene: the Hallstatt cycle and its consequence for grand minima and maxima. *Astr. Astrophys.*, 587:A150, March 2016.

[27] I. G. Usoskin and G. A. Kovaltsov. Production of cosmogenic ^{7}Be isotope in the atmosphere: Full 3-D modeling. *J. Geophys. Res.*, 113(D12):D12107, June 2008.

[28] Ilya G. Usoskin, Galina A. Bazilevskaya, and Gennady A. Kovaltsov. Solar modulation parameter for cosmic rays since 1936 reconstructed from ground-based neutron monitors and ionization chambers. *J. Geophys. Res.: Space Phys.*, 116(A2):A02104, 2011.

[29] R. Vainio, L. Desorgher, D. Heynderickx, M. Storini, E. Flückiger, R. B. Horne, G. A. Kovaltsov, K. Kudela, M. Laurenza, S. McKenna-Lawlor, H. Rothkaehl, and I. G. Usoskin. Dynamics of the Earth's particle radiation environment. *Space Sci. Rev.*, 147:187–231, 2009.

[30] W. R. Webber, P. R. Higbie, and K. G. McCracken. Production of the cosmogenic isotopes ^{3}H, ^{7}Be, ^{10}Be, and ^{36}Cl in the Earth's atmosphere by solar and galactic cosmic rays. *Journal of Geophysical Research (Space Physics)*, 112(A11):A10106, October 2007.

[31] W.R. Webber and P.R. Higbie. Production of cosmogenic be nuclei in the earth's atmosphere by cosmic rays: Its dependence on solar modulation and the interstellar cosmic ray spectrum. *J. Geophys. Res.*, 108:1355, 2003.